

Measurement of the electrical properties of a thundercloud through muon imaging by the GRAPES-3 experiment.

B. Hariharan, A. Chandra, S.R. Dugad, S.K. Gupta,* P. Jagadeesan, A. Jain, P.K. Mohanty, S.D. Morris, P.K. Nayak, P.S. Rakshe, K. Ramesh, B.S. Rao, L.V. Reddy, and M. Zuberi
Tata Institute of Fundamental Research, Homi Bhabha Road, Mumbai 400005, India[†]

Y. Hayashi and S. Kawakami
Graduate School of Science, Osaka City University, Osaka, Japan[†]

S. Ahmad
Aligarh Muslim University, Aligarh 202002, India[†]

H. Kojima, A. Oshima, and S. Shibata
College of Engineering, Chubu University, Kasugai, Aichi, Japan[†]

Y. Muraki
Institute for Space-Earth Environmental Research, Nagoya University, Nagoya, Aichi Japan[†]

K. Tanaka
Graduate School of Information Sciences, Hiroshima City University, Hiroshima, Japan[†]

The GRAPES-3 muon telescope located in Ooty, India records rapid (~ 10 min) variations in the muon intensity during major thunderstorms. Out of a total of 184 thunderstorms recorded during the interval April 2011–December 2014, the one on 1 December 2014 produced a massive potential of 1.3 GV. The electric field measured by four well-separated (up to 6 km) monitors on the ground was used to help estimate some of the properties of this thundercloud including its altitude and area that were found to be 11.4 km above mean sea level (amsl) and ≥ 380 km², respectively. A charging time of 6 min to reach 1.3 GV implied the delivery of a power of ≥ 2 GW by this thundercloud that was moving at a speed of ~ 60 km h⁻¹. This work possibly provides the first direct evidence for the generation of GV potentials in thunderclouds that could also possibly explain the production of highest energy (100 MeV) γ -rays in the terrestrial γ -ray flashes.

Thunderstorms are a spectacular manifestation of the discharge of massive electric potentials that develop in thunderclouds during severe weather conditions. The first authoritative study of thunderstorms by Franklin dates back to 1750s [1]. A major advance in their understanding occurred in 1920s when their dipole structure was identified [2]. However, actual structure is more complex. The separation of electric charges in thunderclouds occurs when supercooled water-droplets make grazing contact with hail-pellets (graupel) polarized by the fine-weather electric field (120 V m⁻¹) on Earth's surface. The rebounding droplets acquire positive charge and are carried by convective updraft toward the cloud-top while negatively charged graupel fall toward cloud-base due to gravity. This creates a vertical field that increases polarizing charge on graupel thus, accelerating this process and reinforcing vertical field, that grows exponentially until air insulation breaks down and triggers a lightning discharge. [3]. Since the thickness of thunderclouds extends to several kilometers, potentials of ≥ 1 GV could be generated [2].

A unique signature of massive electric potentials gen-

erated in thunderclouds was the discovery of terrestrial γ -ray flashes (TGFs) containing MeV photons by the BATSE instrument aboard Compton γ -ray observatory. The source of TGFs was identified to be thunderstorms in the lower tropical atmosphere [4]. The detection of highest γ -ray energy of 100 MeV by the AGILE satellite would however, require bremsstrahlung of very high-energy electrons and presence of potentials of hundreds of MV [5]. The maximum thunderstorm potential measured in balloon soundings is only 0.13 GV [6], well short of the magnitude needed to produce 100 MeV γ -rays [5] and of 1 GV predicted by Wilson [2]. MeV γ -rays produced in thunderstorms have been detected on the ground, both through triggered and natural lightning discharges, showing a close connection of the TGFs detected from space and from ground [7, 8]. Early studies of the changes in muon intensity (I_μ) at low-energies (90 MeV) were shown to be correlated with the electric field of thunderstorms [9, 10] and confirmed by the results from Mt. Norikura [11] and elsewhere [12].

The GRAPES-3 muon telescope (G3MT) in Ooty (11.4° N, 2200 m amsl) studies astrophysics of cosmic rays (CRs) through the measurement of I_μ produced by CRs. Its detection element is a proportional counter (PRC) made from steel pipes ($6\text{m} \times 0.1\text{m} \times 0.1\text{m}$). The G3MT consists of 4 PRC layers under a 2 m thick concrete-roof, resulting in a threshold of $E_\mu = 1 \text{ sec}(\theta) \text{ GeV}$, for muons of zenith angle $= \theta$. This

*gupta.crl@gmail.com

[†]The GRAPES-3 Experiment, Cosmic Ray Laboratory, Raj Bhavan, Ooty 643001, India

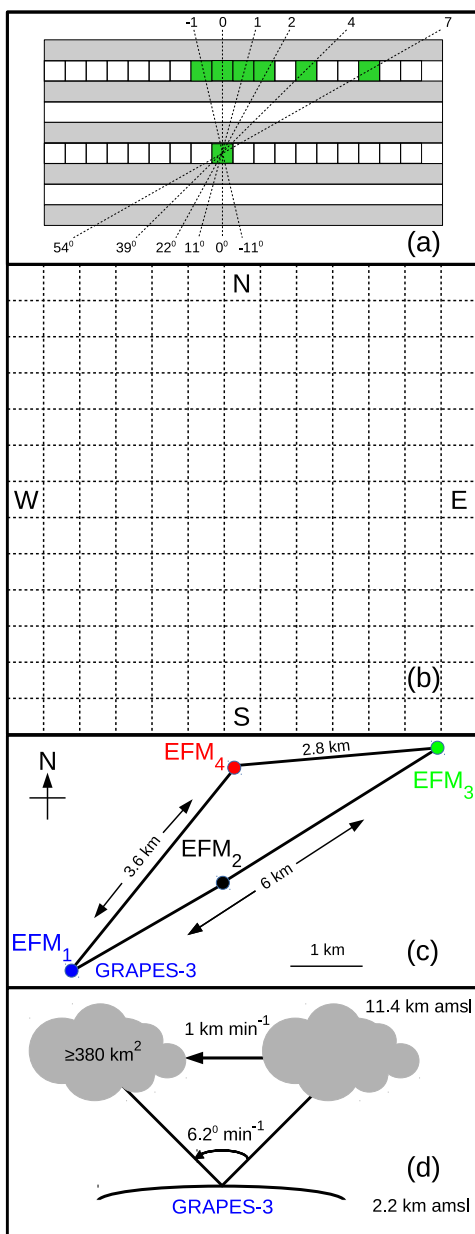


Figure 1: (a) Reconstruction of muon directions in a single projection plane from PRC geometry, (b) telescope field of view (FOV) of 2.3 sr segmented into $13 \times 13 = 169$ directions, (c) locations of EFMs labeled 1 to 4. Maximum distance of EFM_1 and $\text{EFM}_3 = 6$ km, (d) Schematic of thundercloud movement (linear and angular velocities), altitude and area.

4-layer configuration enables muon reconstruction in two mutually perpendicular planes and the two PRC layers in same projection plane separated by ~ 50 cm permit muon direction to be measured with $\sim 4^\circ$ accuracy as shown in Fig. 1a. Thus, the G3MT measures I_μ in 169 directions over a field of view, hereafter $\text{FOV} = 2.3$ sr as shown in Fig. 1b. Although, the solid angle of 169 directions differ significantly, but the area of thundercloud covered varies by only 19% [13]. Since $\sim 2.5 \times 10^6$ muons are recorded every minute, I_μ gets measured to 0.1% precision [14, 15].

During thunderstorms, G3MT detects rapid changes (~ 10 min) in I_μ . Since the muon energies exceed 1 GeV, the presence of large electric potentials is implied. To

probe this phenomenon, electric field monitors, hereafter “EFM” (Boltek model EFM-100 [16]) were installed in April 2011 at four locations, at GRAPES-3, and three others a few km away as shown in Fig. 1c. The data collected during April 2011–December 2014 showed that 184 thunderstorms were detected both by G3MT and EFMs. The seven largest events with muon intensity variation $\Delta I_\mu \geq 0.4\%$ were shortlisted. However, except for the event on 1 December 2014 discussed here, the EFM profiles of remaining six events were extremely complex, that made association of ΔI_μ and electric field of a specific thundercloud difficult.

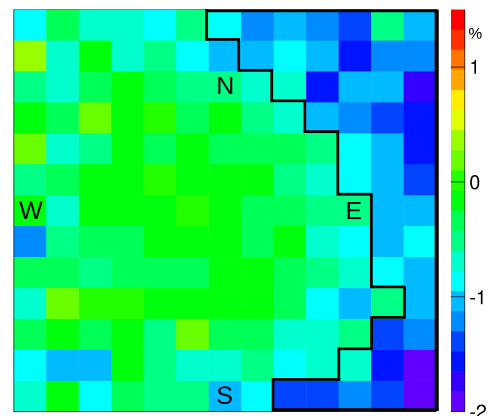


Figure 2: Muon intensity variation during 18 min thunderstorm. 45 out of 169, thunderstorm affected contiguous directions are enclosed by dark boundary. Color-coded % variation shown by a bar on right. Thundercloud angular size in N-S = 74.6° .

Thunderclouds are known to have a complex multipolar structure [3], but here it is assumed to be dipolar since the implications of such a structure can be easily simulated and a quantitative comparison of simulation output with experimental data could be used to obtain the average properties of the thundercloud by treating it as a parallel plate capacitor that can only provide an approximate estimate of its properties. To simulate muon response to thundercloud potential \mathbf{V} , a uniform vertical electric field \mathbf{E}_i for the following three cloud thicknesses \mathbf{D}_i were investigated, where $\mathbf{V} = \mathbf{E}_i \mathbf{D}_i$. (1) $\mathbf{D}_1 = 2$ km for field between 8 and 10 km amsl, (2) $\mathbf{D}_2 = 7.8$ km for field between the ground and 10 km amsl, (3) $\mathbf{D}_3 = 10$ km for field between 10 and 20 km amsl. The dependence of ΔI_μ on \mathbf{V} was obtained from Monte Carlo simulations, described in the next paragraph and was found to be same for cases (1) and (2). For case (3) ΔI_μ was 15% smaller than cases (1) and (2). Thus, the case (3) apart from being unrealistic, also required potentials higher than other two cases. Thus, a uniform electric field applied between 8 and 10 km was used to provide a conservative estimate of the thundercloud potential \mathbf{V} .

The conversion of observed ΔI_μ into equivalent potential \mathbf{V} is derived from Monte Carlo simulations using the CORSIKA code [17], that in turn relies on the choice of hadronic interaction generators. Here, FLUKA [18] and SIBYLL [19] were used for the low- (< 80 GeV) and high-energy (> 80 GeV) interactions, re-

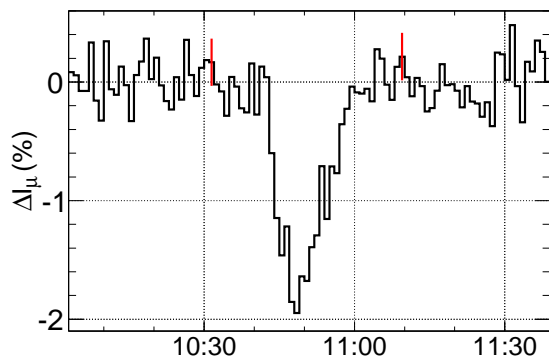


Figure 3: Maximum muon intensity variation $\Delta I_\mu = -2\%$, starting 10:42 UT, lasting 18 min seen during thunderstorm of 1 December 2014. Vertical bars represent $\pm 1\sigma$ errors.

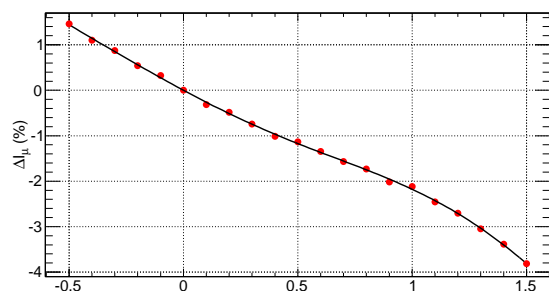


Figure 4: Dependence of ΔI_μ on electric potential (GV) across atmospheric layer 8–10 km amsl, based on simulations for 45 directions shown in Fig. 2.

spectively. When two other popular high-energy generators, namely, QGSJet [20] or EPOS [21] were used, an identical dependence of ΔI_μ on \mathbf{V} was obtained. This is because the affected muons are produced by low-energy (<80 GeV) CRs where the high-energy generators are not used. But, when the other two low-energy generators, GHEISHA [22] or URQMD [23] were used significant differences were observed. Compared to FLUKA, \mathbf{V} inferred for GHEISHA was on an average 15% higher, and for URQMD 6% higher. FLUKA was chosen as it provided the lowest and therefore, the most conservative estimate of the thundercloud potential. Next, the Monte Carlo simulation of muons detected by the G3MT in each of the 169 directions were carried out, first with $\mathbf{V}=0$, and then by applying a \mathbf{V} in the range -3 GV to 3 GV in 0.1 GV steps over a height from 8 to 10 km amsl as explained above. For each direction, the number of muons above the corresponding threshold energy were calculated. A high-statistics muon database of 10^7 for $\mathbf{V}=0$, and 10^6 muons for each non-zero \mathbf{V} was created. This allowed the simulated ΔI_μ to be measured to 0.1% accuracy, much smaller than the error of 0.4 – 2.7% in real data.

The solar-wind introduces a diurnal variation in I_μ that was removed by modeling with a higher-order polynomial after excluding thunderstorm affected 18 min data. The change in I_μ during 18 min is shown in Fig. 2. A cluster of 45 contiguous directions enclosed by dark-boundary displays significant decrease in I_μ as shown in Fig. 3. During 10:42–10:59 UT, a decrease of 2% is visible to the right of the dark boundary in Fig. 2 with a 20σ significance.

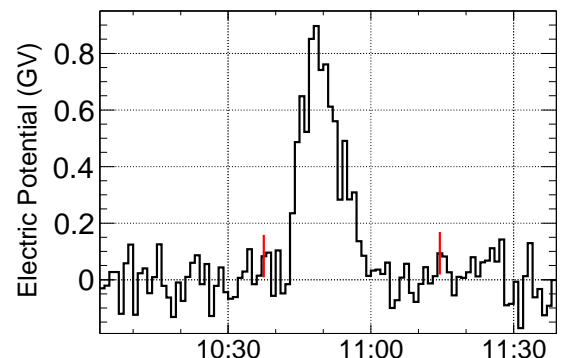


Figure 5: Estimated electric potential shows a maximum of (0.90 ± 0.08) GV at 10:48 UT on 1 December 2014. Vertical bars represent $\pm 1\sigma$ error.

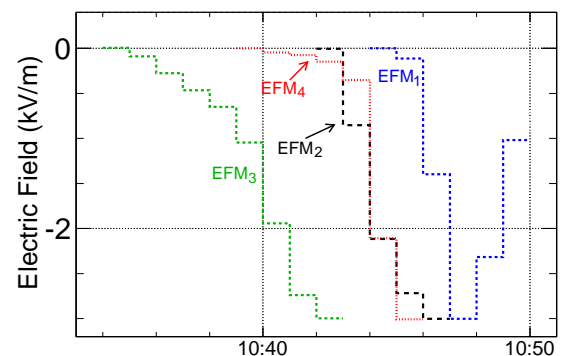


Figure 6: EFM₃ profile appears first, followed by EFM₂ and EFM₄ after a 4 min delay. EFM₁ comes last, 6 min after EFM₃. Based on these EFM delays and locations from Fig. 1c, a thundercloud velocity of 1 km min^{-1} from east to west shown schematically in Fig. 1d is inferred.

Simulated dependence of I_μ for 45 directions on applied potential \mathbf{V} is shown in Fig. 4. A positive \mathbf{V} at thundercloud top relative to bottom would lead to energy-loss $e\mathbf{V}$ for μ^+ and gain $e\mathbf{V}$ for μ^- . Since ratio $\mu^+/\mu^- > 1.0$, the loss of detected μ^+ exceeds the gain of μ^- . Thus, the sum of muons of both polarities decreases for positive \mathbf{V} and beyond 1 GV the slope gradually increases due to rapid increase in decay probability of μ^+ as seen in Fig. 4. This dependence is used to convert the measured ΔI_μ into equivalent \mathbf{V} that peaks at (0.90 ± 0.08) GV as shown in Fig. 5.

The EFM records of electric field (sample rate = 20 s^{-1}) show a smooth profile with an r.m.s. = 0.01 kV m^{-1} in all four cases, same as the EFM resolution. This suggests the absence of major lightning. Hereafter, mean electric field (min^{-1}) is used for comparison with muon data (min^{-1}). Since all EFM profiles were similar and their amplitudes varied 22% around a mean = 3.3 kV m^{-1} , they were normalized to 3 kV m^{-1} as shown in Fig. 6. EFM₃ after a delay of 4 min was followed by EFM₂ and EFM₄, both of which overlapped. EFM₁, closest to G3MT was delayed by 6 min relative to EFM₃, indicating a thundercloud velocity of $\sim 1 \text{ km min}^{-1}$, moving from EFM₃ toward EFM₁ as shown schematically in Fig. 1d.

Thundercloud movement in FOV may be studied by the displacement of its muon image (ΔI_μ) in short 2 min exposures. Because short exposures reduce muon statis-

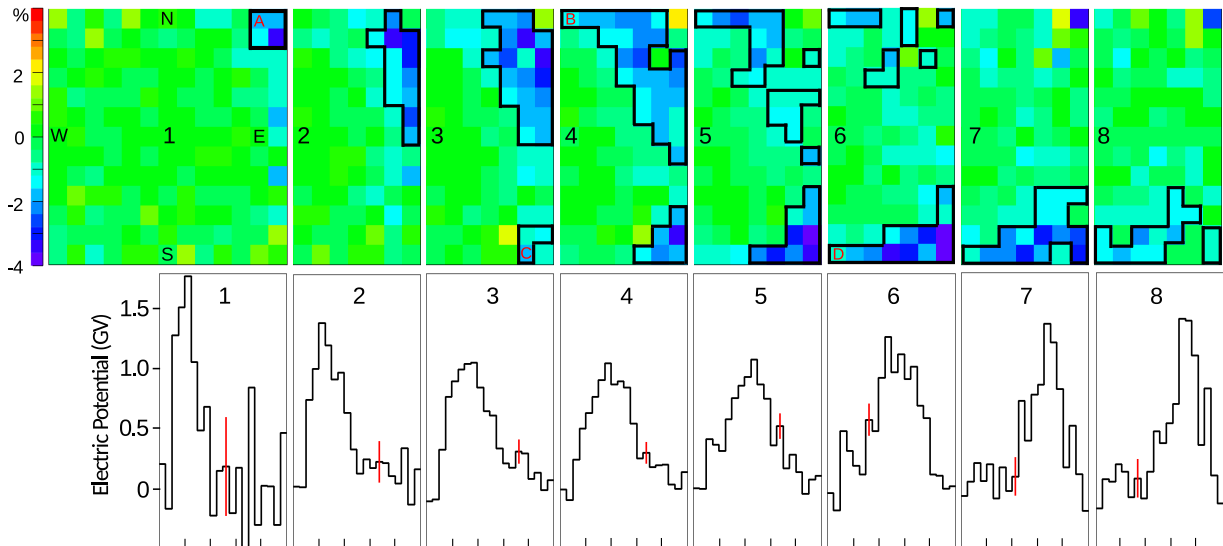


Figure 7: Top 8 panels show affected directions for successive 2 min exposures starting 1 December 2014 10:42 UT. Bottom 8 panels show estimated potentials needed to reproduce ΔI_μ shown in the corresponding panel above for a 20 min duration (10:41–11:00 UT). Maximum potentials of 1.8, 1.4, 1, 1, 1.1, 1.2, 1.3, 1.4 GV (mean = 1.3 GV) observed for panels, 1 through 8. Angular velocity of $6.2^\circ \text{min}^{-1}$, inferred for directions (i) **A** to **B**, (ii) **C** to **D** in north and south FOVs, respectively are shown in Fig. 1d. Vertical bar in each bottom panel corresponds to $\pm 1\sigma$ error.

tics thus, regions that showed (I_μ) decrease, (a) in contiguous directions or, (b) isolated directions over ≥ 2 successive exposures were selected. In Fig. 7, ΔI_μ for first exposure starting 10:42 UT is shown for full FOV in first top-panel labeled 1. A decrease in 4 directions enclosed by dark-boundary is visible, the potential needed is shown in bottom-panel 1 of Fig. 7 that shows a maximum $V = 1.8$ GV during 10:41–11:00 UT. From the second panel onward, only 91 affected directions in the east are displayed. In top-panel 2, 12 affected directions require a maximum $V = 1.4$ GV. This decreases to 1 GV for panels 3 (23) and 4 (32). Then it increases to 1.1 GV and 1.2 GV for panels 5 (28) and 6 (23), respectively. Finally, reaches 1.4 GV for panels 7 (16) and 8 (13). Integer values in the parenthesis next to each panel-number indicate the number of affected directions, highlighted by dark-boundary in the corresponding top-panels.

Successive panels in Fig. 7 show the west boundary of the muon image moving from east-to-west in north-FOV. For example, it moved from direction **A** in top-panel 1 to **B** in top-panel 4 in 6 min implying an angular velocity of $6.2^\circ \text{min}^{-1}$ as depicted in Fig. 1d. A movement of $6.2^\circ \text{min}^{-1}$ of the muon image is seen in south-FOV from **C** to **D** in top-panels 3 and 6, respectively. A similar movement is also reflected in the progressive shift of peak voltage in the eight bottom-panels of Fig. 7. If this angular velocity ($6.2^\circ \text{min}^{-1}$) is combined with linear velocity (1 km min^{-1}) from EFMs, then a height of 11.4 km amsl is obtained, comparable to typical thundercloud height (12 km) [3]. The 1 km min^{-1} velocity and 11.4 km height is consistent with the velocity and height of subtropical jet stream in south India [24].

In north-south direction the muon image covers the full FOV that corresponds to an angular size of 74.6° as seen in Fig. 2. This implies a radius of ≥ 11 km, very similar to average thundercloud radius (~ 12 km) [25] and yields total area of this thundercloud of $\geq 380 \text{ km}^2$. A

thundercloud with infinitesimally thin charged regions, separated by 2 km acts as a parallel-plate capacitor of capacitance $\geq 1.7 \mu\text{F}$. But in reality thickness of charged regions is comparable to their separation that reduces capacitance by $\sim 50\%$ to $\geq 0.85 \mu\text{F}$. $V = 1.3$ GV would require total charge $Q = \geq 1100$ Coulomb and energy of ≥ 720 GJ stored in this thundercloud. A 1.3 GV potential across the thundercloud with its two charged regions of thickness 2 km each and a distance of 2 km between them implies an average field of 2.2 kV cm^{-1} which is lower than the breakdown field at high altitudes [3]. The mean time to reach the maximum potential shown in eight bottom panels in Fig. 7 is 6 min. Thus, the thundercloud would have delivered a power of ≥ 2 GW, comparable to single biggest nuclear reactors [26], hydroelectric and thermal power generators [27]. Separation of 2 km used is reasonable since it extends the thundercloud top into tropopause that defines the limit of cumulonimbus clouds producing major thunderstorms in the atmosphere [3]. Since the capacitance, total charge, energy stored and power delivered by a thundercloud vary inversely with the separation of its charged layers, thus these parameters can be easily calculated for any other separation.

The potential can be measured by integrating electric field over thundercloud height. However, in general the field measured by instruments aboard aircraft and balloons span a region much smaller than the thundercloud height and therefore, can not provide a reliable estimate of the potential. On the other hand, the parameter ΔI_μ depends on the thundercloud potential and is virtually independent of its electric field and/or height. This makes muon telescopes with GeV threshold such as the G3MT ideal for measuring GV potentials in thunderclouds. However, such high-potentials can not be indefinitely sustained and a breakdown of air would result in acceleration of electrons to GeV energies. It

is conceivable that bremsstrahlung emission from GeV electrons could produce photons ranging from a few to beyond 100 MeV in a short flash of terrestrial γ -rays.

Conclusions.— The GRAPES-3 muon telescope is well-suited to measure the electric potential developed in thunderclouds as shown for the 1 December 2014 event where a peak electric potential of 1.3 GV was measured. This value is an order of magnitude larger than the previously reported maximum of 0.13 GV. This possibly is the first direct evidence for the generation of GV potentials in thunderclouds, consistent with the prediction of C.T.R. Wilson, 90 years ago [2]. The existence of GV potentials could explain the production of highest energy γ -rays in terrestrial γ -ray flashes discovered 25 years back [4]. It is shown that a ≥ 2 GW of power, comparable to single biggest nuclear reactors [26], hydroelectric and thermal power generators [27] was delivered by this thunderstorm that was estimated to be moving at speed of 60 km h^{-1} near the top of the troposphere. Despite a simplified structure of the thundercloud used

here, the present work provides reasonable insights into the physical state of the thunderstorms.

Acknowledgments

D.B. Arjunan, V. Jeyakumar, S. Kingston, K. Manjunath, S. Murugapandian, S. Pandurangan, B. Rajesh, K. Ramadass, V. Santhoshkumar, M.S. Shareef, C. Shobana, R. Sureshkumar are thanked for assistance in running the GRAPES-3 experiment. The GRAPES-3 experiment was built with generous support of TIFR and the department of atomic energy, government of India. This work was partially supported by the grants from ISEE, Nagoya University, the Chubu University, and the Ministry of Education and Science, Japan. We thank the three anonymous referees whose prompt, critical and constructive comments led to a significant improvement in the final manuscript and its early publication.

-
- [1] B. Franklin, Experiments and Observations on Electricity made at Philadelphia in America (London, 1751); B. Franklin, Phil. Trans. **47**, 565 (1752).
- [2] C.T.R. Wilson, Nucl. J. Franklin Inst. **208**, 1 (1929); Proc. Phys. Soc. Lond. **37**, 32D (1924); Proc. R. Soc. Lond. A **236**, 297 (1956).
- [3] B.J. Mason, Proc. R. Soc. Lond. A **327**, 433 (1972); ibid **415**, 303 (1988); J. Mason and N. Mason, Eur. J. Phys. **24**, S99 (2003); E.R. Williams, Sci. Am. **259**, 88 (1988); C.P.R. Saunders, Space Sci. Rev. **137**, 335 (2008).
- [4] G.J. Fishman et. al, Science **264**, 1313 (1994).
- [5] M. Tavani et. al, Phy. Rev. Lett. **106**, 018501 (2011).
- [6] T.C. Marshall and M. Stolzenburg, J. Geophys. Res. **106**, 4757 (2001).
- [7] J.R. Dwyer et. al, Science **299**, 694 (2003).
- [8] R. Ringuette et. al, J. Geophys. Res. **118**, 7841 (2013).
- [9] V.V. Alexeenko et al., Proc. 20th International Cosmic Ray Conf. **4**, 272 (1987).
- [10] L.I. Dorman et. al, J. Geophys. Res. **108**, 1181 (2003).
- [11] Y. Muraki et al. Phys. Rev. D **69**, 123010 (2004).
- [12] A. Chilingarian et al. Sci. Rep. **7**, 1371 (2017).
- [13] B. Hariharan et al. Proc. Sci. PoS (ICRC2017) 481.
- [14] S.K. Gupta et al. Nucl. Instrum. Methods A **540**, 311 (2005); Y. Hayashi et al. Nucl. Instrum. Methods A **545**, 643 (2005).
- [15] P.K. Mohanty et al. Phys. Rev. Lett. **117**, 171101 (2016); P.K. Mohanty et al. Phys. Rev. D **97**, 082001 (2018).
- [16] https://www.boltek.com/EFM-100C_Manual_121415.pdf
- [17] <https://www.ikp.kit.edu/corsika>
- [18] <http://www.fluka.org/references.html>
- [19] E.J. Ahn, R. Engel, T.K. Gaisser, P. Lipari, and T. Stanev, Phys. Rev. D **80**, 094003 (2009).
- [20] N.N. Kalmykov, S.S. Ostapchenko, and A.I. Pavlov, Nucl. Phys. B Proc. Suppl. **52B**, 17 (1997).
- [21] T. Pierog et al., arXiv:1306.0121 [hep-ph] (2013).
- [22] <http://cds.cern.ch/record/162911/files/CM-P00055931.pdf>
- [23] <http://urqmd.org>
- [24] <https://www.britannica.com/science/subtropical-jet-stream>
- [25] http://www.nssl.noaa.gov/primer/tstorm/tst_basics.html
- [26] I. Pioro and R. Duffey, ASME J. of Nucl. Rad. Sci. **1**, 011001 (2015).
- [27] <https://www.power-technology.com/features/feature-the-10-biggest-hydroelectric-power-plants-in-the-world>; <https://www.power-technology.com/features/feature-giga-projects-the-worlds-biggest-thermal-power-plants>.